Comb-assisted cavity ring-down spectroscopy of a buffer-gas-cooled molecular beam

Comb-assisted cavity ring-down spectroscopy of a buffer-gas-cooled molecular beam

Luigi Santamaria,[a,b] Valentina Di Sarno,[a,b] Paolo De Natale,[c,d] Maurizio De Rosa,[a,b] Massimo Inguscio,[c] Simona Mosca,[a] Iolanda Ricciardi,[a,b] Davide Calonico,[e] Filippo Levi,[e] and Pasquale Maddaloni*[a,b]

We demonstrate continuous-wave cavity ring-down spectroscopy of a partially hydrodynamic molecular beam emerging from a buffer-gas-cooling source. Specifically, the $(\nu_1+\nu_3)$ vibrational overtone band of acetylene (C_2H_2) around 1.5 μm is accessed using a narrow-linewidth diode laser stabilized against a GPS-disciplined rubidium clock via an optical frequency comb synthesizer. As an example, the absolute frequency of the R(1) component is measured with a fractional accuracy of $\sim 1\cdot 10^{-9}$. Our approach represents the first step towards the extension of more sophisticated cavity-enhanced interrogation schemes, including saturated absorption cavity ring-down or two-photon excitation, to buffer-gas-cooled molecular beams.

1 Introduction

Cold molecular beams, traditionally produced by supersonic jet expansion, have been employed since the early days of spectroscopy in order to suppress Doppler broadening and concentrate the particles in the lowest vibration-rotation levels, thus greatly improving the quality of the absorption spectrum [1–3]. A new impetus to this research field is coming from the recent technologies for generating and manipulating beams of cold stable molecules, buffer-gas cooling (BGC) [4–7], Stark [8–10] and Zeeman [11–13] deceleration above all. Besides having already the strength to dramatically influence the study of new dynamics in low-energy collisions [14] and the accurate control of chemical reactions [15,16], these novel beam sources also serve as the starting point for further cooling and trapping stages. In this respect, opto-electrical cooling [17,18], laser chilling [19,20], and magneto-optical trapping [21,22] represent the most promising candidates to approach the quantum degeneracy regime for the exploration of new Bose-Einstein condensation features or quantum computing issues [23]. In parallel, thanks to the tremendous progress recently experienced in the field of high-resolution spectroscopy and absolute frequency metrology [24], equally disruptive searches, like that of the electric dipole-moment (EDM) of the electron [25,26], the time variation of fundamental constants [27,28] or the parity violation in chiral molecules [29], can be pursued exploiting the new potential of molecular beams. Particularly, by virtue of its applicability to nearly all species and its efficiency in producing very dense samples, the BGC method offers unique perspectives for low-temperature precision molecular spectroscopy. However, so far, only electronic molecular transitions have been addressed on BGC beams, either by laser-induced fluorescence (LIF) [4,30–32] or resonance-enhanced multi-photon ionization (REMPI) [33], whereas spectroscopy of the weaker but much narrower ro-vibrational transitions is still restricted to samples within the BGC cell [34].

In this Letter, we fill this gap by demonstrating the applicability of a high-resolution and high-sensitivity detection technique, like cavity ring-down spectroscopy (CRDS), on a BGC molecular beam. By virtue of its key role in different research areas [35], encompassing fundamental quantum chemistry, atmospheric chemistry, astrophysics, as well as absolute frequency metrology, acetylene is chosen as the test molecule. Specifically, the performance of our scheme is evaluated for a 10-K C_2H_2 beam on the $g\rightarrow(\nu_1+\nu_3)$ R(1) component at 1.5-μm wavelength [36,37]; in particular, due to the frequency-comb-synthesizer referencing of the probe laser, an uncertainty as low as 330 kHz is achieved in the absolute determination of the line center. Being applicable nearly to all kinds of molecules in a variety of wavelength regions, our approach overcomes two major drawbacks of the REMPI technique, namely the applicability to a restricted class of molecular species and the relatively low spectral resolution. Also, in contrast to LIF spectroscopy, typically confined to ultravi-

[a] *CNR-INO, Istituto Nazionale di Ottica, Via Campi Flegrei 34, 80078 Pozzuoli, Italy. E-mail: pasquale.maddaloni@ino.it*
[b] *INFN, Istituto Nazionale di Fisica Nucleare, Sez. di Napoli, Complesso Universitario di M.S. Angelo, Via Cintia, 80126 Napoli, Italy*
[c] *CNR-INO, Largo Fermi 6, 50125 Firenze, Italy*
[d] *INFN, Istituto Nazionale di Fisica Nucleare, Sez. di Firenze, Via G. Sansone 1, 50019 Sesto Fiorentino, Italy*
[e] *INRIM, Istituto Nazionale di Ricerca Metrologica, Strada delle Cacce 91, 10135 Torino, Italy*

olet or visible transitions, the access to vibrational spectra is gained.

2 Experimental setup

The experimental setup, shown in Fig. 1, consists of two main blocks: the BGC source and the laser spectrometer. Described in detail in previous works[38], the heart of the BGC machine is represented by a two-stage pulse tube (PT) cryocooler (Cryomech, PT415) housed in a stainless-steel vacuum chamber and fed with liquid helium by a compressor. The first (second) PT stage yields a temperature of 45 K (4.2 K) provided that its heat load is kept below 40 W (1.5 W); to guarantee this, each plate is enclosed in a gold-plated copper shield (equipped with optical accesses to allow the laser beam propagation). Capillary filling, regulated upstream by two flow controllers with an accuracy of 0.05 sccm (1 sccm$= 4.5\cdot 10^{17}$ molec/s), is used to convey from room-temperature bottles both the acetylene and helium flux, $f_{C_2H_2}$ and f_{He}, respectively, into the BGC cell. This latter consists of a copper cube of side length $l = 3$ cm, in thermal contact with the 4.2-K plate and with a rectangular exit slit ($a_x = 1$ mm, $a_y = 8$ mm). Inside the BGC cell, both translational and internal degrees of freedom of the C_2H_2 molecules are cooled, via collisions, down to the temperature of the He thermal bath, T. To keep the pressure within the radiation shields below 10^{-7} mbar, as required for the formation of the molecular beam, the internal surface of the inner shield is covered with a layer of activated charcoal that, below 15 K, acts as a pump (with a speed of a few thousands $dm^3\cdot s^{-1}$) for helium and non-guided molecules (the gas adsorbed by the charcoal is released during warm up of the cryogenic system and then pumped out of the vessel by a turbo-molecular pump). As a result of the BGC process followed by the expansion through the cell orifice, an acetylene beam at temperature T is created along the z direction with a mean longitudinal speed governed by the Reynolds number, *Rey*. In our case, this can be expressed as[6]

$$Rey \simeq \frac{4\, f_{He}\, \sigma_{He-He}}{a_x} \sqrt{\frac{\pi\, m_{He}}{k_B\, T}}\,, \tag{1}$$

where m_{He} is the He mass and $\sigma_{He-He} \simeq 3\cdot 10^{-19}$ m^2 the elastic cross section for cold He collisions[39]. For $T \simeq 10$ K and $f_{He} < 15$ sccm, $Rey \leq 100$ is found, which allows to estimate the mean longitudinal speed as[6]

$$\bar{v}_z \simeq 1.4 \sqrt{\frac{8 k_B T}{\pi m_{He}}} \sqrt{1 - 4\, Rey^{-4/5}}\,. \tag{2}$$

Concerning the spectrometer, the laser source is a continuous-wave (CW) external-cavity diode laser delivering about 30 mW of power between 1470 and 1570 nm with a free-running emission linewidth less than 50 kHz at 5 μs (TopticaPhotonics, DLC CTL 1520). The laser output beam is split into two main parts. One portion is beaten against the Nth tooth of an optical frequency comb synthesizer (OFCS) (MenloSystems, FC-1500-250-WG) to provide a note at frequency ν_{beat}. This latter is phase-locked by a dedicated electronic servo to a given local oscillator value ($\nu_{LO} = 30$ MHz) by feeding back proper corrections to the laser external-cavity piezo transducer. The second portion passes through a fiber acousto-optic modulator (AOM) whose first-diffracted order is eventually injected into the high-finesse cavity. In this way, the laser emission frequency is determined as[40]

$$\nu_{laser} = \nu_{ceo} + N\nu_r + \nu_{beat} + \nu_{AOM} \tag{3}$$

where ν_{AOM} (80 MHz) is the frequency of the signal driving the AOM, while ν_{ceo} (20 MHz) and ν_r (250 MHz) denote the comb carrier-envelope offset and mode spacing, respectively. The link to the Cs-clock standard is established by stabilizing both ν_{ceo} and ν_r against a high-quality 10-MHz quartz oscillator which is disciplined, in turn, by a Rb/GPS clock; the same reference chain is used to lock the time base of the frequency synthesizers generating the signals at ν_{LO} and ν_{AOM}, respectively. Finally, the integer N is determined, through Eq. (3), by measuring the laser frequency with a 0.2-ppm-accuracy wavelength meter. In this way, the absolute frequency of the laser radiation can be monitored by simultaneously counting the frequencies ν_{ceo}, ν_r and ν_{beat} in Eq. (3). Then, tuning of ν_{laser} across the molecular resonance is accomplished by varying ν_r in discrete steps (at a given N). For each ν_{laser} value, the acetylene absorption is recorded according to a CW CRDS scheme[41,42]. For this purpose, the laser beam is coupled to an enhancement optical resonator consisting of two facing high-reflectivity spherical mirrors (3 m radius of curvature, 1 inch diameter) at a distance of $D = 65$ cm along the x axis. Each mirror is held within the mount against a large-diameter o-ring, which permits angular adjustment of the mirror while maintaining a gas seal; a brass backing ring fits onto the back surface of the mirror, providing a contact point for the ball tips of the alignment screws. The resonator length is continuously dithered by an annular piezoelectric actuator mounted on the input mirror. As a resonance builds up, a threshold detector switches the AOM off; the subsequent ring-down decay is detected by a transimpedence amplified InGaAs photodetector (5 MHz electrical bandwidth). The average of 50 acquisitions, recorded by the oscilloscope, is then used to extract τ by means of a LABVIEW® least-squares fitting routine. In the presence of a molecular resonance, the absorption coefficient $\alpha(\nu)$ is then recovered through the relation[43]

$$\alpha(\nu, z) = \frac{1}{c}\left[\frac{1}{\tau(\nu)} - \frac{1}{\tau_e}\right]\frac{D}{d_x(z)} \equiv \alpha'(\nu)\,\frac{D}{d_x(z)}\,, \tag{4}$$

where $d_x(z)$ is the molecular beam diameter along the x axis

(i.e. the laser propagation direction) at the z coordinate, c the speed of light, and $\tau_e \simeq 10\ \mu$s the empty-cavity decay constant corresponding to a finesse $\mathscr{F} = (\pi c \tau_e)/D \simeq 14000$. The observed absorption profile, $\alpha'(\nu)$, is then fitted by a Gaussian distribution

$$G(\nu) = G_0 \exp\left[-\frac{4\ln 2\,(\nu-\nu_0)^2}{w^2}\right], \tag{5}$$

where the amplitude G_0, the transition center frequency ν_0, and the Doppler width

$$w = \frac{\nu_0}{c}\sqrt{\frac{8\ln 2 k_B T}{m}}, \tag{6}$$

represent the fitting parameters, with m denoting the molecular mass. Subsequently, the temperature of the molecular beam, T, is obtained through Eq. (6).

3 Results and discussion

Fig. 2 shows the CRDS absorption signal at a distance $z_1 = 1$ cm from the BGC cell exit, obtained for $f_{C_2H_2} = 5$ sccm and $f_{He} = 10$ sccm. In these conditions, the temperature measured for the C_2H_2 beam is $T = (13.2 \pm 0.5)$ K, corresponding to $Rey \simeq 60$ and hence to $\bar{v}_z \simeq 340$ m/s. The center frequency of the $(\nu_1+\nu_3)$ R(1) ro-vibrational line is measured as $\nu_0 = (196696652.0 \pm 0.8)$ MHz.

From this signal, the angular divergence of the molecular beam can also be estimated as follows. The starting point is to simulate the trajectories of the molecules escaping from the BGC cell, in order to reconstruct the beam shape at z_1. To this aim, a biased Maxwell-Boltzmann velocity distribution with uniform spatial density is first assumed on the exit slit ($z = 0$),

$$n_{MB}(v_x, v_y, v_z) \propto \exp\left[-\frac{m v_x^2}{2k_B T}\right] \cdot \exp\left[-\frac{m v_y^2}{2k_B T}\right] \cdot \exp\left[-\frac{m(v_z-\bar{v}_z)^2}{2k_B T}\right]. \tag{7}$$

Afterwards, a single molecule is extracted with random velocity (within n_{MB}) and position, (within the exit slit rectangle) and made to follow a rectilinear trajectory with these initial conditions; its position is then calculated as a function of the z coordinate. This procedure is repeated for a huge number ($\sim 10^5$) of particles, which allows to retrieve the transverse profile of the molecular beam along z (see Fig. 3). This yields, in particular, $d_x(z_1) \simeq 0.2$ cm (root mean square), corresponding to a full angular divergence of $\Delta\phi = 2 \cdot \arctan[d_x(z_1)/z_1] \simeq 23^\circ$.

Then, we can calculate the average molecular density (along x) at z_1, $\bar{n}(z_1)$, using the following formula,

$$\bar{n}(z_1)\frac{S}{w} \simeq \alpha(\nu_0, z_1) = \alpha'(\nu_0)\frac{D}{d_x(z_1)}, \tag{8}$$

where $S \simeq 0.9 \cdot 10^{-19}$ cm/molec is the linestrength of the $(\nu_1+\nu_3)$ R(1) ro-vibrational line at $T \simeq 13.2$ K[38] and $w \simeq 100$ MHz is the Doppler width extracted by the fit. Finally, with reference to Fig. 4, from $\bar{n}(z_1) \simeq 1.6 \cdot 10^{12}$ molec/cm^3 and denoting with $\rho \simeq 670\ \mu$m the laser beam waist in the high-finesse cavity, we estimate the molecular beam flux as $\mathscr{Z} \simeq \bar{n}(z_1)\bar{v}_z \rho\, d_x(z_1) \simeq 7.1 \cdot 10^{14}$ molec/s.

To test the validity of our spectroscopic approach at greater distances from the BGC source, the cavity ring-down signal is also measured at $z_2 = 10$ cm for the same ro-vibrational transition, as shown in Fig. 5. In this case, higher flux values are used ($f_{C_2H_2} = 40$ sccm and $f_{He} = 10$ sccm) to obtain a signal-to-noise ratio of SNR $\simeq 7$. The center frequency of the molecular resonance is now shifted of about -8 MHz from the value obtained above ($\nu_0 = 196696652.0$ MHz); such a disagreement is attributable to a distortion of the Doppler absorption profile which occurs when a higher acetylene input flux is used. In these conditions, indeed, the clogging of the BGC cell exit hole (due to the sticking of the molecules) is so fast that the output molecular flux, and hence the absorption signal strength, decreases as the laser frequency sweeps along the resonance. As experimentally verified, the resulting asymmetry in the absorption profile leads to a shift downwards (upwards) of the center frequency when the molecular resonance is scanned from lower to higher (higher to lower) frequencies. Moreover, as expected, due to the increased heat load against a limited cooling power of the cryogenic source, larger fluxes also lead to wider Doppler absorption profiles, namely to higher beam temperatures. Nevertheless, as deducible from Fig. 5, at sufficiently large distances from the BGC cell exit, even for such high fluxes ($f_{C_2H_2} = 40$ sccm and $f_{He} = 10$ sccm), a Doppler width corresponding to a temperature as low as 16 K is obtained for the molecular beam; this is due to the presence of the inner shield that encloses the 4.2-K pulse tube plate, which eliminates the most peripheral parts of the beam, providing a sort of skimmer effect. This seems to suggest that the molecular beam is, in fact, the superposition of several portions (along the x direction), all at the same temperature, but each with its own velocity x component. Accordingly, skimming the molecular beam spatially filters out, in the distribution of individual collisionally boosted velocities, the most peripheral contributions, namely the ones with largest Doppler shifts, thus resulting in a lower effective transverse temperature. The above discussion points to the necessity of working with low flux values. In this sense, shown in Fig. 6 is a measurement performed for $f_{C_2H_2} = 4$ sccm and $f_{He} = 8$ sccm, this time with a 2-mm-diameter circular escape hole. By virtue of the significantly improved *SNR*, the center frequency of the $(\nu_1+\nu_3)$ R(1) ro-vibrational line is now measured with a fractional accuracy of $1.5 \cdot 10^{-9}$. Therefore, CRDS measurements at $z_2 = 10$ cm for $f_{C_2H_2} = 4$ sccm and $f_{He} = 8$ sccm with the aid of superior high-reflectivity mirrors

are planned for the next future.

The accuracy in the absolute frequency measurement demonstrated here can be far improved after a realistic refinement of both the molecular beam figures and the laser spectrometer performance. Indeed, much room for progress can come from optimization of the injection of $f_{C_2H_2}$ and f_{He} as well as of the geometrical parameters of the BGC cell in order to increase the output beam flux, while reducing its temperature and divergence. On the other side, we can work towards a more robust cavity design (also including top-quality mirrors) to be employed within an interrogation scheme with superior spectral resolution, like saturated absorption cavity ring-down (SCAR)[44].

4 Conclusions

In conclusion, we believe that our scheme represents, in several respects, a big step forward for high-precision spectroscopy on cold molecular beams. Firstly, combination of cavity-enhanced spectroscopy with the relatively high sample densities achievable for all types of molecules with buffer gas cooling allows to greatly increase the number of species that can be studied, compared to REMPI. A second key aspect resides in having earned an effective and versatile tool to study vibrational transitions on BGC beams, as opposed to LIF. Thirdly, in view of highly accurate spectroscopic frequency measurements, the absence of intense electric fields acting on the molecules dramatically suppresses troublesome systematic effects. In the near future, further developments can come from the implementation of other cavity-enhanced advanced interrogation schemes, like direct frequency comb spectroscopy[45,46]. As for metrology applications, a state-of-the-art optical frequency standard, as delivered by an actively stabilized fiber link[47], is being finalized; its combination with the present BGC setup together with an ultra-high-resolution spectroscopic interrogation technique, like two-photon excitation in the optical domain[27,48], may produce new sets of ultra-precise frequency measurements on cold molecules at the electronVolt energy scale.

The authors acknowledge technical support by G. Notariale and fruitful discussions with G. Santambrogio. This work was funded by MIUR-FIRB project RBFR1006TZ and by INFN project SUPREMO.

References

1 *Atomic and Molecular Beam Methods*, ed. G. Scoles, D. Bassi, U. Buck and D. C. Laine, Oxford University Press, 1988, vol. 1.

2 *Atomic and Molecular Beam Methods*, ed. G. Scoles, D. C. Laine and U. Valbusa, Oxford University Press, 1992, vol. 2.

3 Demtröder, *Laser Spectroscopy*, Springer, 4th edn., 2008, vol. 2: Experimental techniques.

4 S. E. Maxwell, N. Brahms, R. deCarvalho, D. R. Glenn, J. S. Helton, S. V. Nguyen, D. Patterson, J. Petricka, D. DeMille and J. M. Doyle, *Physical Review Letters*, 2005, **95**, 173201.

5 C. Sommer, L. D. van Buuren, M. Motsch, S. Pohle, J. Bayerl, P. W. H. Pinkse and G. Rempe, *Faraday Discussions*, 2009, **142**, 203.

6 N. R. Hutzler, H.-I. Lu and J. M. Doyle, *Chemical Reviews*, 2012, **112**, 4803.

7 N. E. Bulleid, S. M. Skoff, R. J. Hendricks, B. E. Sauer, E. A. Hinds and M. R. Tarbut, *Physical Chemistry Chemical Physics*, 2013, **15**, 12299.

8 H. L. Bethlem, G. Berden and G. Meijer, *Physical Review Letters*, 1999, **83**, 1558.

9 S. Y. T. van de Meerakker, H. L. Bethlem and G. Meijer, *Nature Physics*, 2008, **4**, 595.

10 S. Y. T. van de Meerakker, H. L. Bethlem, N. Vanhaecke and G. Meijer, *Chemical Reviews*, 2012, **112**, 4828.

11 A. W. Wiederkehr, H. Schmutz, M. Motsch and F. Merkt, *Molecular Physics*, 2012, **110**, 1807.

12 M. Motsch, P. Jansen, J. A. Agner, H. Schmutz and F. Merkt, *Physical review A*, 2014, **89**, 043420.

13 P. Jansen, L. Semeria and F. Merkt, *Journal of Molecular Spectroscopy*, 2016, **322**, 9.

14 B. K. Stuhl, M. T. Hummon and J. Ye, *Annual Review of Physical Chemistry*, 2014, **65**, 501.

15 T. Softley and M. Bell, *Molecular Physics*, 2009, **107**, 99.

16 H. Sassmannshausen, F. Merkt and J. Deiglmayr, *Physical Review Letters*, 2015, **114**, 133201.

17 M. Zeppenfeld, B. G. U. Englert, R. Glöckner, A. Prehn, M. Mielenz, C. Sommer, L. D. van Buuren, M. Motsch and G. Rempe, *Nature*, 2012, **491**, 570.

18 A. Prehn, M. Ibrügger, R. Glöckner, G. Rempe and M. Zeppenfeld, *Physical Review Letters*, 2016, **116**, 063005.

19 E. S. Shuman, J. F. Barry and D. DeMille, *Nature*, 2010, **467**, 820.

20 T. A. Isaev and R. Berger, *Physical Review Letters*, 2016, **116**, 063006.

21 M. T. Hummon, M. Yeo, B. K. Stuhl, A. L. Collopy, Y. Xia and J. Ye, *Physical Review Letters*, 2013, **110**, 143001.

22 E. B. Norrgard, D. J. McCarron, M. H. Steinecker, M. R. Tarbutt and D. DeMille, *Physical Review Letters*, 2016, **116**, 063004.

23 L. D. Carr, D. DeMille, R. V. Krems and J. Ye, *New Journal of Physics*, 2009, **11**, 055049.

24 P. Maddaloni, M. Bellini and P. De Natale, *Laser-based measurements for time and frequency applications. A handbook*, Taylor & Francis Group, 2013.

25 J. J. Hudson, D. M. Kara, I. J. Smallman, B. E. Sauer, M. R. Tarbutt and H. E. A., *Nature*, 2011, **473**, 493.

26 J. Baron, W. C. Campbell, D. DeMille, J. M. Doyle, G. Gabrielse, Y. V. Gurevich, P. W. Hess, N. R. Hutzler, E. Kirilov, I. Kozyryev, B. R. O'Leary, C. D. Panda, M. F. Parsons, E. S. Petrik, B. Spaun, A. C. Vutha and A. D. West, *Science*, 2013, **343**, 269.

27 A. Shelkovnikov, R. J. Butcher, C. Chardonnet and A. Amy-Klein, *Physical Review Letters*, 2008, **100**, 150801.

28 W. Ubachs, J. Bagdonaite, E. J. Salumbides, M. T. Murphy and L. Kaper, *arXiv:1511.04476*, 2016.

29 S. K. Tokunaga, C. Stoeffler, F. Auguste, A. Shelkovnikov, C. Daussy, A. Amy-Klein, C. Chardonnet and B. Darquié, *Molecular Physics*, 2013, **111**, 2363.

30 M. Stoll, J. M. Bakker, T. C. Steimle, G. Meijer and A. Peters, *Physical Review A*, 2008, **78**, 032707.

31 M. Yeo, M. T. Hummon, A. L. Collopy, B. Yan, B. Hemmerling, E. Chae, J. M. Doyle and J. Ye, *Physical Review Letters*, 2015, **114**, 223003.

32 J. F. Barry, E. S. Shuman and D. DeMille, *Physical Chemistry Chemical Physics*, 2011, **13**, 18936.

33 D. Patterson, J. Rasmussen and J. M. Doyle, *New Journal of Physics*,

2009, **11**, 055018.

34 B. Spaun, P. Bryan Changala, D. Patterson, B. J. Bjork, O. H. Heckl, J. M. Doyle and J. Ye, *arXiv:1601.07845*, 2016.

35 M. Herman, *Molecular Physics*, 2007, **105**, 2217.

36 B. Amyay, M. Herman, A. Fayt, A. Campargue and S. Kassi, *Journal of Molecular Spectroscopy*, 2011, **267**, 116.

37 B. Amyay, A. Fayt, M. Herman and J. Vander Auwera, *Journal of Physical and Chemical reference Data*, in press.

38 L. Santamaria, V. Di Sarno, I. Ricciardi, M. De Rosa, S. Mosca, G. Santambrogio, P. Maddaloni and P. De Natale, *The Astrophysical Journal*, 2015, **801**, 50.

39 L. Santamaria, V. Di Sarno, I. Ricciardi, S. Mosca, M. De Rosa, G. Santambrogio, P. Maddaloni and P. De Natale, *Journal of Molecular Spectroscopy*, 2015, **300**, 116.

40 P. Maddaloni, P. Cancio and P. De Natale, *Measurement Science and Technology*, 2009, **20**, 052001.

41 D. Romanini, I. Ventrillard, G. Méjean and E. Kerstel, in *Cavity-Enhanced Spectroscopy and Sensing*, ed. G. Gagliardi and H.-P. Loock, Springer-Verlag Berlin Heidelberg, 2014, vol. 179, ch. Introduction to Cavity Enhanced Absorption Spectroscopy.

42 P. Maddaloni, P. Malara, E. De Tommasi, M. De Rosa, I. Ricciardi, G. Gagliardi, F. Tamassia, G. Di Lonardo and P. De Natale, *The Journal of Chemical Physics*, 2010, **133**, 154317.

43 G. Berden, R. Peeters and G. Meijer, *International Reviews in Physical Chemistry*, 2000, **19**, 565.

44 I. Galli, S. Bartalini, R. Ballerini, M. Barucci, P. Cancio, M. De Pas, G. Giusfredi, D. Mazzotti, N. Akikusa and P. De Natale, *OPTICA*, 2016, in press.

45 F. Adler, M. J. Thorpe, K. C. Cossel and J. Ye, *Annual Review of Analytical Chemistry*, 2010, **3**, 175.

46 M. Siciliani de Cumis, R. Eramo, N. Coluccelli, M. Cassinerio, G. Galzerano, P. Laporta, P. De Natale and P. Cancio Pastor, *Physical Review A*, 2015, **91**, 012505.

47 D. Calonico, E. K. Bertacco, C. E. Calosso, C. Clivati, G. A. Costanzo, M. Frittelli, A. Godone, A. Mura, N. Poli, D. V. Sutyrin, G. Tino, M. E. Zucco and F. Levi, *Applied Physics B: Lasers and Optics*, 2014, **117**, 979.

48 C. J. Foot, B. Couillaud, R. G. Beausoleil and T. W. Hänsch, *Physical Review Letters*, 1985, **54**, 1913.

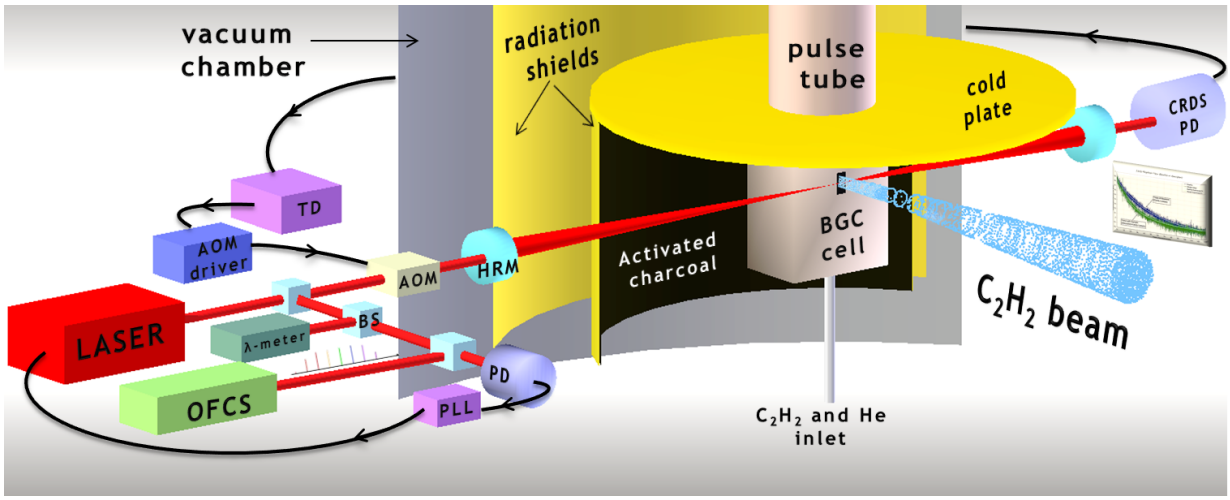

Fig. 1 Layout of the experimental setup consisting of two main blocks: the buffer-gas-cooling source and the comb-referenced laser spectrometer. The following legend holds: HRM=high-reflectivity mirror, TD=threshold detector, PD=photo-detector, PLL=phase locked loop, BS=beam splitter.

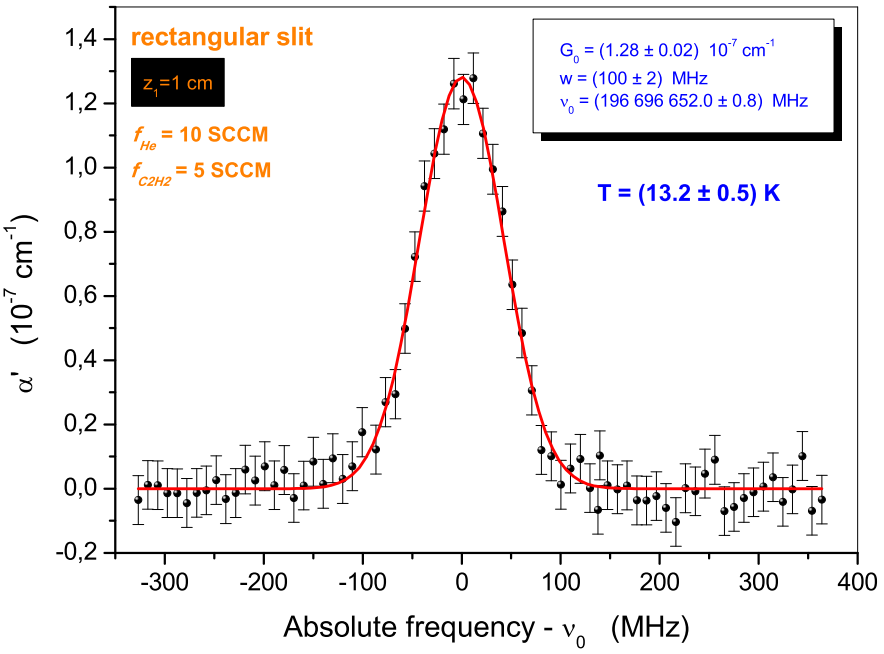

Fig. 2 CRDS signal, with a signal-to-noise ratio of SNR $\simeq 30$, corresponding to $f_{C_2H_2} = 5$ sccm and $f_{He} = 10$ sccm, as measured on the acetylene beam at a distance of $z_1 = 1$ cm from the exit slit of the BGC cell. The center frequency of the $(\nu_1 + \nu_3)$ R(1) ro-vibrational line is measured with a fractional accuracy of $4.1 \cdot 10^{-9}$.

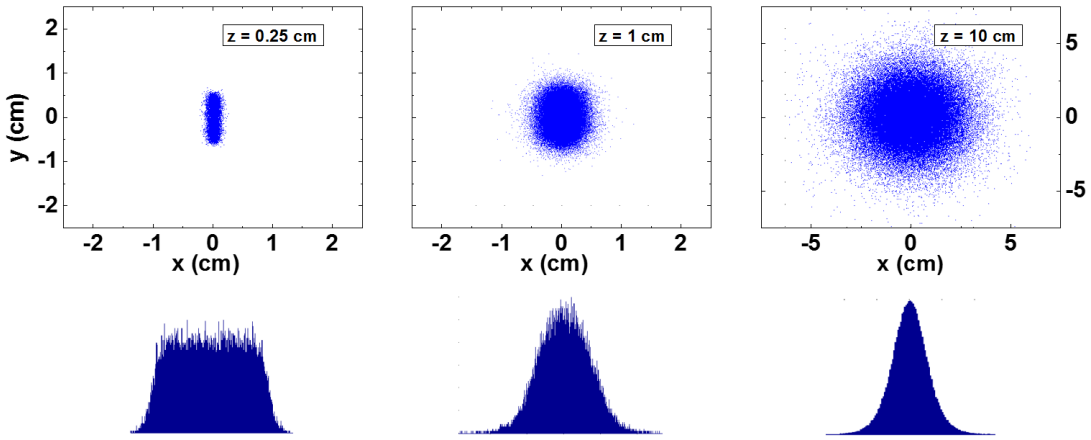

Fig. 3 Simulation of the transverse profile of the molecular beam at different positions along the z axis, carried out for $\bar{v}_z = 340$ m/s and $T = 13.2$ K.

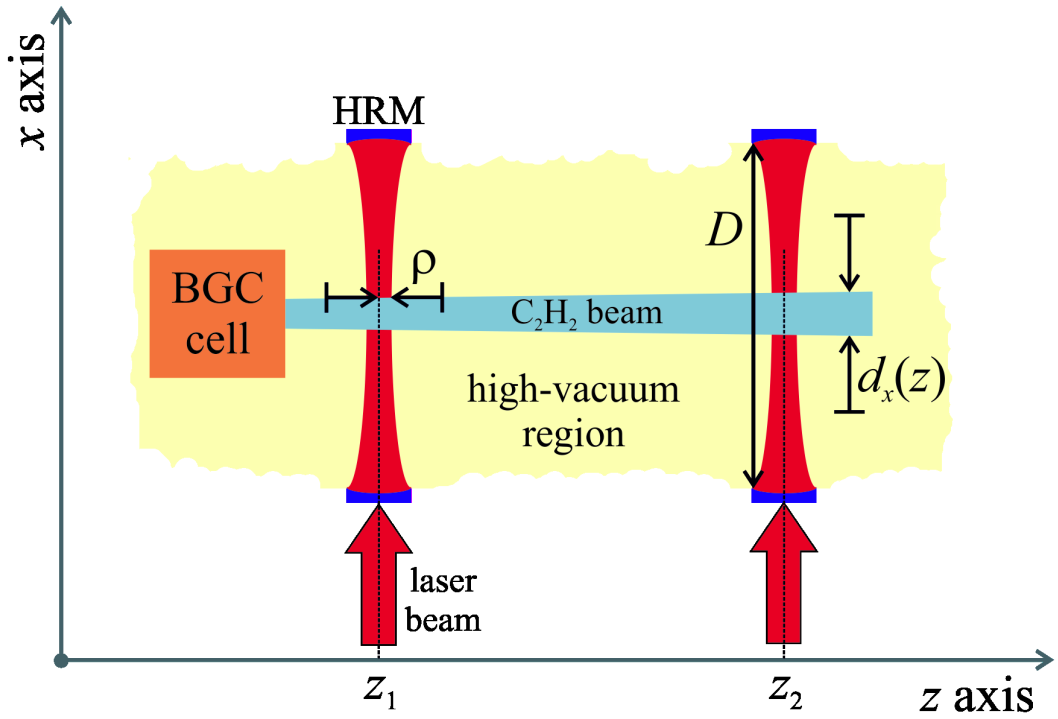

Fig. 4 Schematic topview (not to scale) of the CRDS setup evidencing the relevant geometrical parameters involved in the estimation of the molecular beam density and divergence.

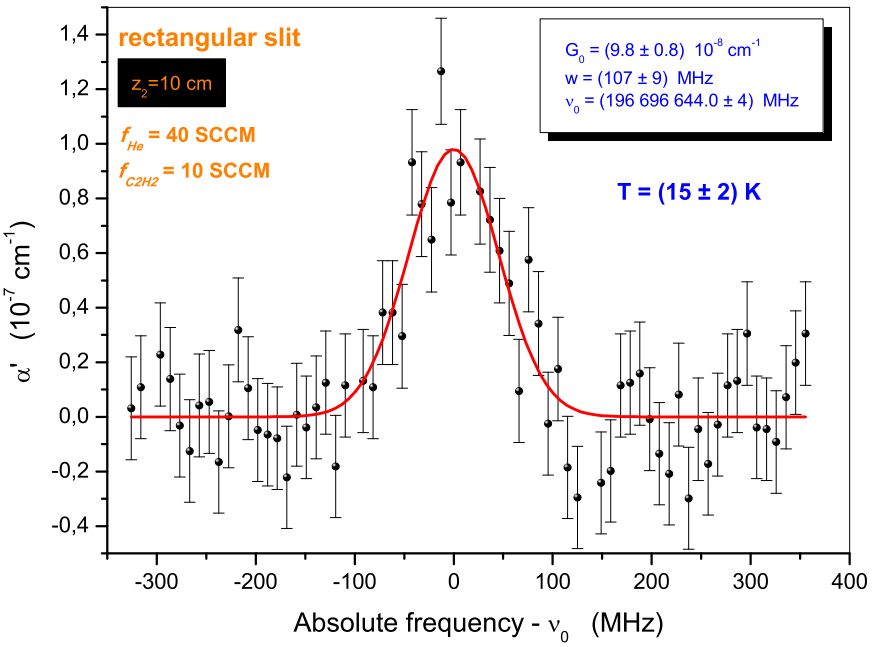

Fig. 5 CRDS signal measured (for the same ro-vibrational transition) on the acetylene beam at a distance $z_2 = 10$ cm from the exit slit of the BGC cell. Here, higher flux values are used ($f_{C_2H_2} = 40$ sccm and $f_{He} = 10$ sccm), leading to a slightly increased beam temperature, $T = (15 \pm 2)$ K, and a larger Reynolds number, $Rey \simeq 220$. This corresponds to a beam longitudinal speed $\bar{v}_z \simeq 1.4\sqrt{\frac{8k_BT}{\pi m_{He}}} = 390$ m/s[6].

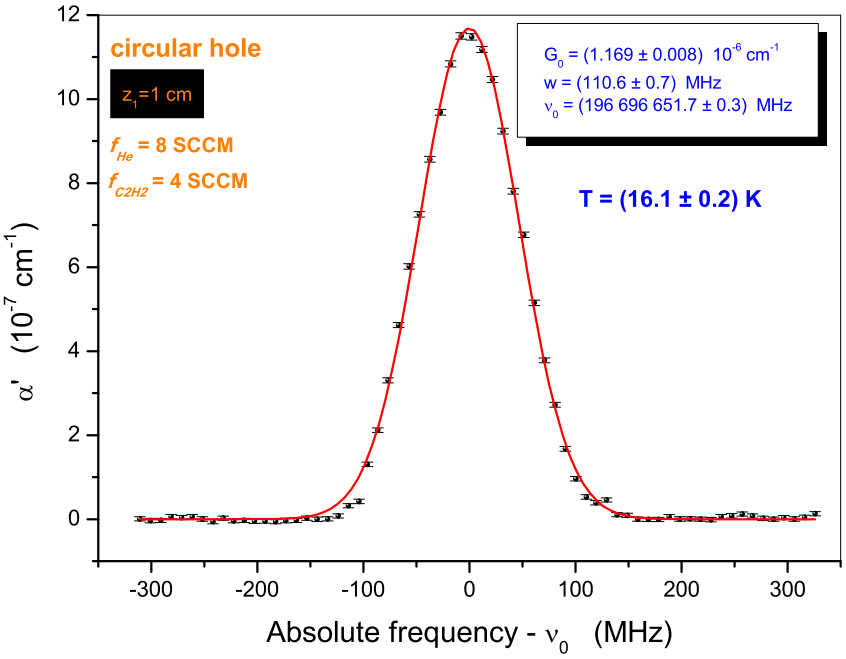

Fig. 6 CRDS signal measured on the acetylene beam for $f_{C_2H_2} = 4$ sccm and $f_{He} = 8$ sccm at a distance of $z_1 = 1$ cm from the BGC cell exit. Here, the escape hole is circular with a diameter of 2 mm. Thanks to the enhanced signal-to-noise ratio ($SNR \simeq 250$), the center frequency of the $(\nu_1 + \nu_3)$ R(1) ro-vibrational line is now measured with a fractional accuracy of $1.5 \cdot 10^{-9}$.